

# Interband photorefraction in $\text{Sn}_2\text{P}_2\text{S}_6$ at visible wavelengths

Roger Mosimann, Daniel Haertle, Mojca Jazbinšek, Germano Montemezzani, and Peter Günter

*Nonlinear Optics Laboratory, Swiss Federal Institute of Technology, Eidgenössische Technische Hochschule Zurich, CH-8093 Zurich, Switzerland*

Received January 1, 2003; revised March 22, 2003; accepted March 22, 2006; posted March 24, 2006 (Doc. ID 67403)

Continuous-wave photorefractive experiments in  $\text{Sn}_2\text{P}_2\text{S}_6$  crystals and interband photorefraction at the visible wavelengths of 514 and 488 nm are presented. Two-wave mixing and Bragg diffraction measurements at 514 nm show grating response times of around 100  $\mu\text{s}$  at moderate light intensities of 0.6 W/cm<sup>2</sup>, i.e., 2 orders of magnitude faster than measured in the same crystal in the conventional photorefractive regime. A large two-wave mixing gain of up to  $\Gamma = 60 \pm 8 \text{ cm}^{-1}$  is measured, and holes are identified as dominant charge carriers for the interband photorefractive effect. © 2006 Optical Society of America

OCIS codes: 090.7330, 160.5320, 190.5330.

## 1. INTRODUCTION

The interband photorefractive effect is characterized by a rapid charge redistribution upon inhomogeneous illumination, followed by an electro-optic change of the optical properties because of the generated space-charge electric field due to band-to-band photoexcitation of intrinsic charge carriers. Compared with the conventional photorefractive effect connected with photoexcitation from deep donor centers, the main advantages of the interband photorefractive effect are a much faster response and a strong robustness of the grating against illumination with sub-bandgap photons.<sup>1,2</sup> For the interband photorefractive effect, intentional doping of the crystal to achieve efficient photocarrier generation from donor levels is not required since carriers are directly excited from intrinsic energy levels of the material. The interband photorefractive effect is attractive for many applications because of the faster recording times. Recording times of less than 100  $\mu\text{s}$  have been reported in  $\text{KNbO}_3$  at 1 mW/cm<sup>2</sup> power levels.<sup>1</sup> Already implemented and demonstrated are incoherent-to-coherent light converters,<sup>3</sup> optical joint Fourier-transform correlators,<sup>4</sup> fast dynamical light-induced waveguides,<sup>5</sup> and tunable optical filters for wavelength division multiplexing.<sup>6</sup>

Interband photorefraction has been studied previously in  $\text{KNbO}_3$  (Ref. 1) and  $\text{LiTaO}_3$ ,<sup>2</sup> where ultraviolet (UV) light was used for the grating recording. For many practical applications, however, it would be more convenient to use visible instead of UV light due to the several advantages in terms of availability of laser sources, standard optical devices, easier detection, etc. The availability of a material with a large electro-optic response that is suitable for interband photorefraction under visible illumination therefore offers interesting perspectives. The material studied in this work, tin hypophosphite ( $\text{Sn}_2\text{P}_2\text{S}_6$ ), fulfills all requirements for fast interband photorefraction at visible wavelengths due to its large electro-optic effects [e.g.,  $r_{111}^T = 174 \text{ pm/V}$  at  $\lambda = 633 \text{ nm}$  (Ref. 7)] and the suitable bandgap energy of  $E = 2.3 \text{ eV}$ .

$\text{Sn}_2\text{P}_2\text{S}_6$  is a monoclinic ferroelectric crystal with a broad transparent region [0.53–8  $\mu\text{m}$  (Ref. 8)]. In the regime of the conventional photorefractive effect, it shows fast photorefractive grating recording times and large refractive index changes in the red and near-infrared region.<sup>9–14</sup> The possibility for fast hologram recording in  $\text{Sn}_2\text{P}_2\text{S}_6$  via interband photorefraction under cw visible illumination was demonstrated recently in preliminary experiments by our group.<sup>15</sup> We have also measured the photoconductivity and determined the absorption coefficients at 488 and 514 nm.<sup>16</sup> In the pulsed regime, effects ascribed to the interband photorefractive effect were already used to demonstrate optical correlation at high repetition frame rates using a wavelength of 532 nm.<sup>4</sup>

In this paper we present photorefractive gratings in  $\text{Sn}_2\text{P}_2\text{S}_6$  with very fast buildup times (less than 100  $\mu\text{s}$ ), recorded at visible green ( $\lambda = 514 \text{ nm}$ ) and blue ( $\lambda = 488 \text{ nm}$ ) light. The diffraction efficiency of a Bragg grating follows an intensity dependence as expected for the interband regime. The strong influence of the orientation of the optical indicatrix in the mirror plane of the monoclinic structure on the observed Bragg diffraction angle is predicted and experimentally verified. This phenomenon can be used to gain information on the material refractive indices within the high absorption region. Finally, two-wave mixing experiments permit us to determine very high effective exponential gain coefficients of up to 60  $\text{cm}^{-1}$  for the wavelength of  $\lambda = 514 \text{ nm}$  as a result of the strong photorefractive and electro-optic nonlinearity. This measurement also allowed us to determine the most mobile charge carriers in  $\text{Sn}_2\text{P}_2\text{S}_6$ .

## 2. EXPERIMENT

### A. Sample Preparation

$\text{Sn}_2\text{P}_2\text{S}_6$  single crystals were produced by the conventional vapor-transport technique<sup>17</sup> using iodine as a transporter. At room temperature  $\text{Sn}_2\text{P}_2\text{S}_6$  has a ferroelectric monoclinic structure with point group  $m$ . In this

work we use the coordinate system as defined in Ref. 18 with the  $z$  axis parallel to the crystallographic  $c$  axis,  $y \parallel b$  normal to the mirror plane, and  $x$  normal to  $y$  and  $z$ . The indicatrix is rotated in the  $xz$  plane, and its rotation angle  $\alpha_{\text{ind}}$  is defined as the angle between the  $x$  axis and the major principal axis of the indicatrix. This angle is wavelength and temperature dependent.<sup>18</sup> The poling was performed by heating the crystal above the second-order phase transition at  $T_C = 338 \pm 2$  K and slowly cooling it down to room temperature with an electric field of  $\sim 1$  kV/cm applied along the  $x$  direction. We used a bulk crystal and a thin  $z$  plate. The dimensions of the thick  $\text{Sn}_2\text{P}_2\text{S}_6$  crystal were  $5.07 \text{ mm} \times 5.38 \text{ mm} \times 4.85 \text{ mm}$  along the  $x$ ,  $y$ , and  $z$  axes, respectively. The thin plate had dimensions of  $7.3 \text{ mm} \times 8.3 \text{ mm} \times 0.045 \text{ mm}$  and was attached to a quartz substrate with a thickness of 3 mm. The single-domain state was verified using the directional light-scattering method described in Ref. 19.

### B. Bragg Diffraction and Two-Wave Mixing

Bragg diffraction from photorefractive gratings was performed in a nondegenerate four-wave mixing configuration in the longitudinal geometry as illustrated in Fig. 1. In this geometry all three beams enter the crystal through the same surface and propagate in the  $x, z$  plane. The experiments were performed with a writing beam from an Ar-ion laser at 514 and 488 nm (Coherent Innova 100, maximum cw single-mode power of 1 W) and a reading beam from a He-Ne laser (maximum cw power of 5 mW). The absorption constant  $\alpha$  at 488 nm is  $2600 \pm 800 \text{ cm}^{-1}$  for the  $x$  polarization and  $1730 \pm 70 \text{ cm}^{-1}$  for the  $y$  polarization; at 514 nm it is  $490 \pm 20 \text{ cm}^{-1}$  for the  $x$  polarization and  $110 \pm 10 \text{ cm}^{-1}$  for the  $y$  polarization.<sup>16</sup>

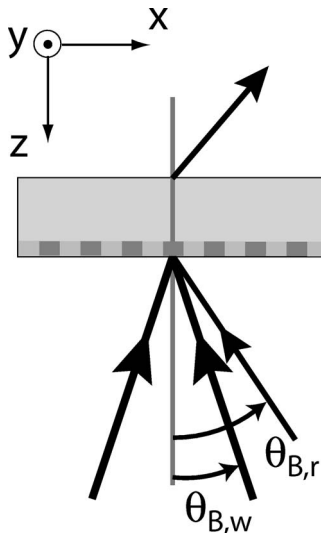


Fig. 1. Experimental configuration and crystal orientation for longitudinal Bragg diffraction measurements. The grating is written by two recording beams at 514 or 488 nm incident symmetrically with respect to the sample normal at angles  $\pm \theta_{B,w}$ . The readout beam at 633 nm is shown on the right side with respect to the sample normal; we refer to this configuration as readout from the right side, corresponding to positive angles  $\theta_{B,r}$ . Readout from the left side, corresponding to negative angles  $\theta_{B,r}$ , means that the readout beam is on the left side with respect to the sample normal, according to the crystal orientation indicated on the scheme.

The recording light penetration depth  $1/\alpha$  is therefore of the order of  $4\text{--}200 \mu\text{m}$  for the wavelengths between  $\lambda = 488$  and  $514 \text{ nm}$ , which means that the interaction length for the readout beam is quite short. The readout beam was  $p$  polarized (in the  $x, y$  plane) in all the measurements, while the writing beams were either  $p$  or  $s$  polarized. The diffracted probe beam (He-Ne laser) had a wavelength of  $\lambda = 633 \text{ nm}$  and thus a photon energy of  $h\nu = 2.0 \text{ eV}$ , which is smaller than the bandgap energy in  $\text{Sn}_2\text{P}_2\text{S}_6$  (2.3 eV). Therefore it is expected that the reading beam cannot influence the interband grating. An acousto-optical deflector was used to turn the recording beam on and off. After the crystal the diffracted beam power was measured with a photodiode.

For the two-wave mixing experiment we used the same setup as for the Bragg diffraction experiments without the readout beam and introduced a filter (1%) to weaken one of the writing beams, which is then called the signal beam. For this experiment we used a thin  $\text{Sn}_2\text{P}_2\text{S}_6$  plate of  $45 \mu\text{m}$  thickness along the  $z$  axis, obtained by polishing down the bulk crystal. After the sample, we focused the beam on the photodiode to collect all the light passing through the absorbing thin plate.

The photoconductivity measurements show that the interband regime, in which the photoconductivity follows a square-root intensity dependence,<sup>1</sup> is reached at intensities above  $1 \text{ mW/cm}^2$  at 488 nm and  $10 \text{ mW/cm}^2$  at 514 nm.<sup>16</sup> In all the experiments in this work we have used higher intensities; therefore we consider that, at the intensity levels used in the present measurements, the main contribution comes from gratings associated with mobile carriers and not carriers from deep traps. In general, deep-trap gratings might be formed deeper inside the crystal where the intensity becomes lower, as observed previously in  $\text{KNbO}_3$  (Ref. 15) and  $\text{LiTaO}_3$ .<sup>2</sup>

## 3. RESULTS AND DISCUSSION

### A. Bragg Diffraction

#### 1. Determination of the Bragg Angle

The external Bragg angle  $\theta_{B,r}$  of the reading beam can be calculated by

$$\sin \theta_{B,r} = \frac{\lambda_r}{\lambda_w} \sin \theta_{B,w} \quad (1)$$

if the writing beams are incident symmetrically to the sample;  $\theta_{B,w}$  is the external incidence angle of the writing beam,  $\lambda_r$  is the readout beam wavelength, and  $\lambda_w$  is the writing beam wavelength. For  $\text{Sn}_2\text{P}_2\text{S}_6$  this equality will in general not hold because the indicatrix is rotated in the  $x, z$  plane and therefore the main axes are not perpendicular to the crystal surface. Additionally this rotation changes with the wavelength ( $\alpha_{\text{ind}}^{514 \text{ nm}} = 39.9^\circ$ ,  $\alpha_{\text{ind}}^{633 \text{ nm}} = 43.3^\circ$ ).<sup>18</sup> We chose  $p$ -polarized readout beams, since the effective electro-optical coefficient is then closer to  $r_{111}^T$ , which is the largest coefficient in this material.<sup>7</sup> This implies, however, that the rotation of the indicatrix has to be taken into account in every measurement, as explained in the following.

Let us first consider the case where the two writing beams are also polarized in the plane of incidence. In this

case the two writing beams have different refractive indices in the crystal and therefore the grating fringes are not perpendicular to the surface of the crystal. This effect modifies the Bragg angle from Eq. (1), and the direction of the Bragg angle shift is determined by the direction of the optical indicatrix with respect to the direction of the incident beams.

In the second case the writing beams are *s* polarized. In this case both writing beams have the same refractive index and the grating fringes are perpendicular to the surface. However, there will still be a shift of the Bragg angle

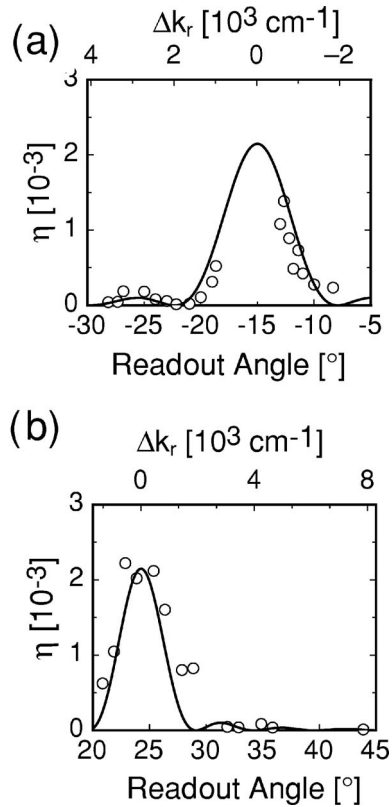


Fig. 2. Diffraction efficiency  $\eta$  as a function of the readout angle and the wave-vector mismatch  $\Delta k$  for (a) readout from the left side and (b) readout from the right side (see Fig. 1). All the writing and readout beams were *p* polarized. The solid curves are given by Eq. (2) using the same parameters for both curves and correspond to a grating thickness  $\tilde{d}=30\ \mu\text{m}$ ,  $\lambda_w=514\ \text{nm}$ ,  $\Delta n=3.0\times 10^{-4}$ ,  $\Lambda=0.94\ \mu\text{m}$ ,  $\theta_{B,r}^{\text{left}}=-15.0^\circ$ , and  $\theta_{B,r}^{\text{right}}=24.3^\circ$ . The total writing intensity was  $I_w=460\ \text{mW/cm}^2$ .

with respect to Eq. (1) due to the *p*-polarized readout beam, for which the refractive index will be different if it comes from the left or from the right side with respect to the sample normal.

Figure 2 shows the measured diffraction efficiency  $\eta$  as a function of the incidence angle  $\theta_{B,r}$  of the readout beam for writing beams polarized in the incidence plane entering at  $\theta_{B,w}=15.9^\circ$ . The measured diffraction efficiency has been approximated with the theoretical dependence obtained for phase-only transmission gratings<sup>20,21</sup>:

$$\eta = \frac{\sin^2(\nu^2 + \xi^2)^{1/2}}{(1 + \xi^2/\nu^2)} \exp(-\alpha d), \quad (2)$$

with

$$\xi^2 = \frac{\Delta k_r^2}{4} \tilde{d}^2, \quad (3)$$

$$\nu^2 = \left\{ \frac{\pi \Delta n \tilde{d}}{\lambda_r [\cos(\theta_i) \cos(\theta_d)]^{1/2}} \right\}^2, \quad (4)$$

where  $d$  is the thickness of the crystal;  $\tilde{d}$  is the thickness of the grating;  $\theta_i$  and  $\theta_d$  are the internal angles of the Poynting vectors of the incoming and diffracted waves, respectively;  $\Delta k_r$  is the wave-vector mismatch, and  $\Delta n$  is the effective refractive index modulation amplitude. Similar measurements have also been performed for *s*-polarized writing beams at  $\lambda=514\ \text{nm}$  and  $\lambda=488\ \text{nm}$ . In Table 1 the values for the external Bragg angles calculated from the known refractive indices<sup>18</sup> and the measured values are presented. The calculation of the Bragg angle is sensitive to the values of the refractive indices, which were extrapolated from Sellmeier parameters obtained from data outside the absorption regime ( $\lambda=550\text{--}2300\ \text{nm}$ ). Nevertheless, the calculated and measured angles match well. This indicates also that the refractive indices can be extrapolated accurately with a Sellmeier formula from Ref. 18 to lower wavelengths until at least 488 nm. The error for the refractive indices used to calculate the Bragg angles is 0.015, resulting from the error in the determination of the Bragg angle of  $1^\circ$ .

The direction of the  $+x$  axis is  $15^\circ$  off the direction of the polar axis (see Fig. 3); the direction of the  $+x$  axis is more difficult to determine.<sup>18</sup> The direction of the shift of the Bragg angle from Eq. (1) can be used to determine the direction of the  $+z$  axis with respect to the entrance sur-

**Table 1. Measured External Bragg Angles  $\theta_{B,r}$  for the *p*-Polarized Readout Beam Compared with the Bragg Angles Calculated by Taking into Account the Rotation of the Indicatrix and without Rotation**

$\lambda$ (nm)	Position of the Readout Beam	Writing Polarization	$\theta_{B,r}$ (deg)		
			Calculation with Eq. (1)	Calculated	Measured
514	Left side	<i>p</i>	-19.6	-14.9	-15.0
514	Right side	<i>p</i>	19.6	24.6	24.3
514	Left side	<i>s</i>	-19.6	-24.1	-24.0
488	Left side	<i>s</i>	-20.8	-25.2	-25.3

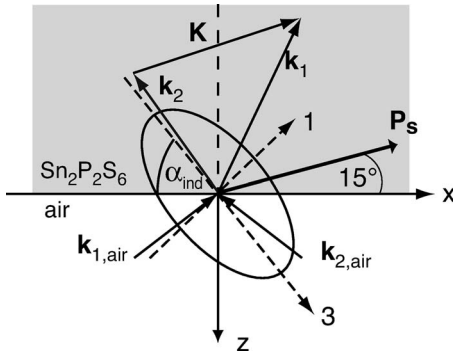


Fig. 3. Orientation of the indicatrix and the  $x$ , and  $z$  axes as determined from the Bragg diffraction measurements. The  $z$  axis is pointing out of the crystal.  $\mathbf{k}_{1,\text{air}}$  and  $\mathbf{k}_{2,\text{air}}$  are the incident writing wave vectors,  $\mathbf{k}_1$  and  $\mathbf{k}_2$  are the wave vectors in the crystal,  $\mathbf{K}$  is the grating vector, and  $\alpha_{\text{ind}}$  is the rotation angle of the indicatrix.

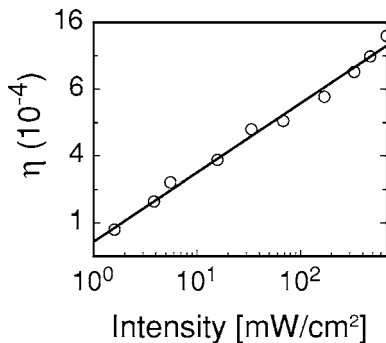


Fig. 4. Intensity dependence of the diffraction efficiency (on a square-root and logarithmic scale). The theoretical line is according to relation (5) with parameters  $\alpha=1730 \text{ cm}^{-1}$  (from Ref. 16),  $\Delta n=1.2 \times 10^{-4}$ ,  $I_{\text{ref}}=0.2 \text{ mW/cm}^2$ . ( $\lambda=488 \text{ nm}$ , writing beams are  $s$  polarized, readout beam is  $p$  polarized. Grating spacing  $\Lambda=0.9 \mu\text{m}$ .)

face. As a recipe, with the  $+x$  axis pointing to the right, the  $+z$  axis is in the backward direction if a larger Bragg angle is measured for a readout beam coming from the right than for one coming from the left. The resulting  $+z$  axis (defined as in Ref. 18) is shown in Fig. 3.

## 2. Intensity Dependence

The dependence of the Bragg diffraction efficiency on the intensity of the writing beam was studied with both  $p$ - and  $s$ -polarized writing beams and at the wavelengths of 488 and 514 nm. The intensity of the writing beams was changed with a filter in front of the crystal and the intensity of the readout beam was  $I_{\text{HeNe}}=130 \text{ mW/cm}^2$ .

The diffraction efficiency defined as the ratio between the diffracted and the incident light intensities is shown in Fig. 4 as a function of intensity for  $\lambda=488 \text{ nm}$  and  $s$  polarization. This relation can be approximated by<sup>1</sup>

$$\sqrt{\eta} \approx \frac{\pi \Delta n}{\lambda \alpha} \ln \left( \frac{I_0}{I_{\text{ref}}} \right), \quad (5)$$

where  $\Delta n$  is the average amplitude of the refractive index change,  $\alpha$  is the absorption constant at the wavelength of the writing beams,  $I_0$  is the total incident writing intensity, and  $I_{\text{ref}}$  is a reference intensity needed for normalization. This behavior is expected if we assume that increas-

ing the writing intensity increases the effective thickness of the grating and that the depth dependence of the grating is a step function. In  $\text{KNbO}_3$  similar interband effects have been observed and the depth dependence was shown to describe the experimental results better than an exponential decrease.<sup>1</sup> The straight line in Fig. 4 is a good indicator that we are in the interband regime.

## 3. Dynamics of the Grating Buildup

One of the main advantages of interband photorefractive effects is the time scale for the buildup of the grating. To measure the dynamics of the buildup we used an acousto-optic deflector with a rise time of less than  $0.5 \mu\text{s}$  to ensure a fast switching of the laser beam. Figure 5 shows the diffraction efficiency of the grating for  $\lambda=633 \text{ nm}$   $p$ -polarized light after turning on the writing  $p$ -polarized beams at  $\lambda=514 \text{ nm}$  and two different total intensities.

The dynamics of the diffraction efficiency cannot be explained with a simple model, because the intensity of the writing beam is exponentially decreasing with the depth inside the crystal. For the buildup of the holographic grating this means that the buildup time, the amplitude, and the phase of the grating will depend on the depth. The diffracted beam at the back side of the crystal is formed by the coherent sum of all the amplitudes of the diffracted light at different depths. For a model with several time constants, the measured curves are not described significantly better than for just one parameter. The buildup was therefore modeled with a semiheuristic exponential function of the form

$$\eta = \eta_1 [1 - \exp(-t/\tau)]^2. \quad (6)$$

This yields a time constant for the grating buildup  $\tau$  (see Fig. 5). For  $320 \text{ mW/cm}^2$  writing beam intensity,  $\tau=125 \mu\text{s}$ ; and for  $650 \text{ mW/cm}^2$ ,  $\tau=80 \mu\text{s}$ , which is faster (as expected) for the higher writing beam intensity.

The measured buildup at  $\lambda=514 \text{ nm}$  where  $\alpha=490 \text{ cm}^{-1}$  is very fast compared with typical buildup times measured in brown  $\text{Sn}_2\text{P}_2\text{S}_6$  at  $\lambda=633 \text{ nm}$  for  $1 \text{ W/cm}^2$ , which is  $\tau=5\text{--}50 \text{ ms}$ . It is also more than 2 orders of magnitude faster than in  $\text{LiTaO}_3$  in the interband regime at approximately the same writing intensity and  $\lambda=257 \text{ nm}$  where  $\alpha=270 \text{ cm}^{-1}$  (Ref. 2); and it is almost as fast as in  $\text{KNbO}_3$ , where buildup times of  $\sim 10 \mu\text{s}$  were ob-

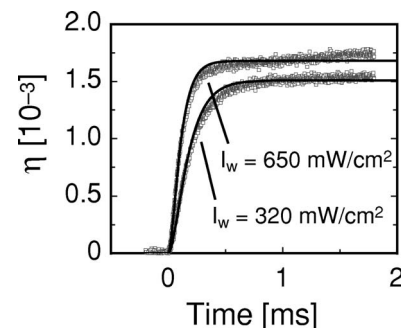


Fig. 5. Grating buildup dynamics for two different writing intensities at  $\lambda=514 \text{ nm}$ . The readout beam intensity was  $130 \text{ mW/cm}^2$ , grating spacing  $\Lambda=1.0 \mu\text{m}$ , and both the readout and writing beams were  $p$  polarized. The solid curves are according to Eq. (6) with the buildup times of  $\tau=125 \mu\text{s}$  for  $320 \text{ mW/cm}^2$  and  $\tau=80 \mu\text{s}$  for  $650 \text{ mW/cm}^2$ .

tained in transversal geometry at  $1\text{ W/cm}^2$  and  $\lambda = 351\text{ nm}$  but with a much higher absorption ( $\alpha = 1900\text{ cm}^{-1}$ ) and with an external applied field for an enhancement of the diffraction efficiency.<sup>22</sup>

### B. Two-Wave Mixing in a Thin Plate

Two-wave mixing experiments in the interband regime allow for the determination of the most mobile charge carriers and the verification of the amplitude of the refractive index change  $\Delta n$ . The experiments were performed in a  $45\text{ }\mu\text{m}$  thick  $\text{Sn}_2\text{P}_2\text{S}_6$  plate, with  $p$ -polarized light of wavelength  $\lambda = 514\text{ nm}$ , a total intensity of  $I_0 = 373\text{ mW/cm}^2$  (pump beam  $= 370\text{ mW/cm}^2$ , signal beam  $= 3\text{ mW/cm}^2$ ), and a grating spacing of  $\Lambda = 1\text{ }\mu\text{m}$ . In the Bragg diffraction experiments described in Subsection 3.A.1 we measured an effective grating thickness of  $\tilde{d} = 30\text{ }\mu\text{m}$  for a similar writing intensity. To simplify the calculation of the two-wave mixing gain, we make an assumption of a constant amplitude grating of the same thickness and for no two-wave mixing interaction below  $\tilde{d} = 30\text{ }\mu\text{m}$ . This is justified by the fact that deeper in the crystal the grating cannot be formed because the dark conductivity dominates over the photoconductivity induced by the not yet absorbed photons. Therefore we can estimate the lower limit of the gain coefficient as

$$\Gamma = \frac{1}{\tilde{d}} \ln \frac{I_{w/\text{pump}}}{I_{w/o\text{ pump}}}, \quad (7)$$

where  $I_{w/\text{pump}}$  and  $I_{w/o\text{ pump}}$  are, respectively, the signal beam intensities with and without the pump beam turned on. The two-wave mixing gain can be related to an effective refractive index change  $\Delta n$  as

$$\Gamma = \frac{4\pi}{\lambda \cos \theta_s} \Delta n, \quad (8)$$

where  $\theta_s$  is the internal incidence angle of the signal wave.

The result of  $\Gamma = 60 \pm 8\text{ cm}^{-1}$  with a grating spacing of  $1\text{ }\mu\text{m}$  shows a very high gain in the visible, and the corresponding refractive index contrast  $\Delta n = (2.4 \pm 0.5) \times 10^{-4}$  corresponds well to the value of  $\Delta n$  calculated from Bragg diffraction in Subsection 3.A.1. In the conventional photorefractive regime at  $\lambda = 633\text{ nm}$ , the maximal gain reaches  $\sim 7\text{ cm}^{-1}$ . The high gain in the interband region can be explained by two factors. First, the number of effective charge carriers  $N_{\text{eff}}(\lambda)$  increases with decreasing wavelength as observed in the transparent region<sup>13</sup>; second, the electro-optic coefficient  $r(\lambda)$  also increases as it approaches the absorption edge.<sup>7</sup>

To verify the true two-wave mixing origin of the energy transfer, we rotated the plate by  $180^\circ$  around the  $y$  axis so that the spontaneous polarization was inverted. In this case we measured a weakening of the signal beam, as expected for photorefractive two-wave mixing. If the signal beam gets amplified with the spontaneous polarization pointing in the direction of the amplification, the most mobile charge carriers are holes, since the corresponding electro-optic coefficient is positive.<sup>7</sup> This is the situation that occurs in  $\text{Sn}_2\text{P}_2\text{S}_6$ , so the main charge carrier is the same as has been identified for conventional

photorefraction.<sup>7,12</sup> In the case of the interband photorefractive effect this implies that  $\mu_h > \mu_e$ , where  $\mu_h$  is the mobility of the holes and  $\mu_e$  is the mobility of the electrons.<sup>1,23</sup>

## 4. CONCLUSIONS

We have investigated and analyzed the interband photorefractive effects in  $\text{Sn}_2\text{P}_2\text{S}_6$  at visible wavelengths. This allowed us to determine an average refractive index change of  $\Delta n = (3 \pm 0.03) \times 10^{-4}$  at  $\lambda = 514\text{ nm}$ . Because of the rotation of the indicatrix, we observed a considerable shift of the Bragg angle, which allowed us to determine the refractive indices in the interband regime and determine the direction of the  $+z$  axis in the crystal.

The buildup time constant of the interband photorefractive effect are of the order of  $100\text{ }\mu\text{s}$  at an intensity of  $0.6\text{ W/cm}^2$  and therefore are more than 2 orders of magnitude shorter than for the conventional photorefractive effect at  $\lambda = 633\text{ nm}$  at the same intensity level. Additionally the effect is observed around  $\lambda = 530\text{ nm}$ , which is easily accessible by compact all-solid-state laser sources.

With a thin plate of  $\text{Sn}_2\text{P}_2\text{S}_6$ , two-wave mixing effects at a wavelength of  $\lambda = 514\text{ nm}$  were demonstrated with a very high gain coefficient of  $\Gamma = 60 \pm 8\text{ cm}^{-1}$  for  $p$ -polarized light. We concluded that the most mobile charge carriers at this wavelength are holes, and therefore  $\mu_h > \mu_e$ .

Interband holography in  $\text{Sn}_2\text{P}_2\text{S}_6$  proves therefore to be an important tool, not only for applications in fast parallel coherent optics, but also as an experimental technique that allows one to access and determine material parameters in the high-absorption region.

## ACKNOWLEDGMENT

We thank J. Hajfler for his expert crystal preparation and A. A. Grabar for supplying the crystals. This research has been supported by the Swiss National Science Foundation.

The present address for G. Montemezzani is Laboratoire Matériau Optiques, Photonique et Systemes (Unité Mixte de Recherche, Centre National de la Recherche Scientifique 7132), University of Metz and Supélec, 57070 Metz, France. The e-mail address for R. Mosimann is roger.mosimann@phys.ethz.ch.

## REFERENCES

1. G. Montemezzani, P. Rogin, M. Zgonik, and P. Günter, "Interband photorefractive effects: theory and experiments in  $\text{KNbO}_3$ ," *Phys. Rev. B* **49**, 2484–2502 (1994).
2. P. Dittrich, B. Koziarska-Glinka, G. Montemezzani, P. Günter, S. Takekawa, K. Kitamura, and Y. Furukawa, "Deep-ultraviolet interband photorefractive effect in lithium tantalate," *J. Opt. Soc. Am. B* **21**, 632–639 (2004).
3. P. Bernasconi, G. Montemezzani, M. Wintermantel, L. Biaggio, and P. Günter, "High-resolution, high-speed photorefractive incoherent-to-coherent optical converter," *Opt. Lett.* **24**, 199–201 (1999).
4. R. Ryf, G. Montemezzani, P. Günter, A. A. Grabar, I. M. Stoika, and Y. M. Vysochanskii, "High-frame-rate joint Fourier-transform correlator based on  $\text{Sn}_2\text{P}_2\text{S}_6$  crystal," *Opt. Lett.* **26**, 1666–1668 (2001).
5. P. Dittrich, G. Montemezzani, P. Bernasconi, and P. Günter, "Fast, reconfigurable light-induced waveguides," *Opt. Lett.* **24**, 1508–1510 (1999).

6. P. Dittrich, G. Montemezzani, and P. Günter, "Tunable optical filter for wave length division multiplexing using dynamic interband photorefractive gratings," *Opt. Commun.* **214**, 363–370 (2002).
7. D. Haertle, G. Caimi, A. Haldi, G. Montemezzani, P. Günter, A. A. Grabar, I. M. Stoika, and Y. M. Vysochanskii, "Electro-optical properties of  $\text{Sn}_2\text{P}_2\text{S}_6$ ," *Opt. Commun.* **215**, 333–343 (2003).
8. D. Haertle, M. Jazbinsek, G. Montemezzani, and P. Günter, "Nonlinear optical coefficients and phase-matching conditions in  $\text{Sn}_2\text{P}_2\text{S}_6$ ," *Opt. Express* **13**, 3765–3776 (2005).
9. S. G. Odoulov, A. N. Shumelyuk, U. Hellwig, R. A. Rupp, A. A. Grabar, and I. M. Stoyka, "Photorefraction in tin hypthiodiphosphate in the near infrared," *J. Opt. Soc. Am. B* **13**, 2352–2360 (1996).
10. A. A. Grabar, I. V. Kedyk, M. I. Gurzan, I. M. Stoika, A. A. Molnar, and Y. M. Vysochanskii, "Enhanced photorefractive properties of modified  $\text{Sn}_2\text{P}_2\text{S}_6$ ," *Opt. Commun.* **188**, 187–194 (2001).
11. A. Shumelyuk, S. Odoulov, D. Kip, and E. Kratizig, "Electric-field enhancement of beam coupling in  $\text{Sn}_2\text{P}_2\text{S}_6$ ," *Appl. Phys. B* **72**, 707–710 (2001).
12. M. Jazbinsek, G. Montemezzani, P. Günter, A. A. Grabar, I. M. Stoika, and Y. M. Vysochanskii, "Fast near-infrared self-pumped phase conjugation with photorefractive  $\text{Sn}_2\text{P}_2\text{S}_6$ ," *J. Opt. Soc. Am. B* **20**, 1241–1246 (2003).
13. M. Jazbinsek, D. Haertle, G. Montemezzani, P. Günter, A. A. Grabar, I. M. Stoika, and Y. M. Vysochanskii, "Wavelength dependence of visible and near infrared photorefraction and phase conjugation in  $\text{Sn}_2\text{P}_2\text{S}_6$ ," *J. Opt. Soc. Am. B* **22**, 2459–2467 (2005).
14. T. Bach, M. Jazbinsek, P. Günter, A. A. Grabar, I. M. Stoika, and Y. M. Vysochanskii, "Self pumped optical phase conjugation at  $1.06\ \mu\text{m}$  in Te-doped  $\text{Sn}_2\text{P}_2\text{S}_6$ ," *Opt. Express* **13**, 9890–9896 (2005).
15. G. Montemezzani, R. Ryf, D. Haertle, P. Günter, A. A. Grabar, I. M. Stoika, and Y. M. Vysochanskii, "Continuous-wave interband photorefractive gratings in  $\text{Sn}_2\text{P}_2\text{S}_6$ ," *Ukr. J. Phys.* **49**, 333–338 (2004).
16. R. Mosimann, D. Haertle, M. Jazbinsek, G. Montemezzani, and P. Günter, "Determination of the absorption constant in the interband region by photocurrent measurements," *Appl. Phys. B* **83**, 115–119 (2006).
17. C. D. Carpentier and R. Nitsche, "Vapour growth and crystal data of the thio(seleno)-hypodiphosphates  $\text{Sn}_2\text{P}_2\text{S}_6$ ,  $\text{Sn}_2\text{P}_2\text{S}_6$ ,  $\text{Pb}_2\text{P}_2\text{S}_6$ ,  $\text{Pb}_2\text{P}_2\text{Se}_6$  and their mixed crystals," *Mater. Res. Bull.* **9**, 401–410 (1974).
18. D. Haertle, A. Guarino, J. Hajfler, G. Montemezzani, and P. Günter, "Refractive indices of  $\text{Sn}_2\text{P}_2\text{S}_6$  at visible and infrared wavelengths," *Opt. Express* **13**, 2047–2057 (2005).
19. A. A. Grabar, "Directional light scattering by domain walls in  $\text{Sn}_2\text{P}_2\text{S}_6$  uniaxial ferroelectrics," *J. Phys.: Condens. Matter* **10**, 2339–2346 (1998).
20. H. Kogelnik, "Coupled wave theory for thick hologram gratings," *Bell Syst. Tech. J.* **48**, 2909–2947 (1969).
21. G. Montemezzani and M. Zgonik, "Light diffraction at mixed phase and absorption gratings in anisotropic media for arbitrary geometries," *Phys. Rev. E* **55**, 1035–1047 (1997).
22. G. Montemezzani, P. Rogin, M. Zgonik, and P. Günter, "Interband photorefractive effects in  $\text{KNbO}_3$  induced by ultraviolet illumination," *Opt. Lett.* **18**, 1144–1146 (1993).
23. M. Carrascosa, F. Agullo-Lopez, G. Montemezzani, and P. Günter, "Photorefractive gratings generated by band-gap excitation: application to  $\text{KNbO}_3$ ," *Appl. Phys. B* **72**, 697–700 (2001).